IEEE Control Systems Letters paper presented at
2023 American Control Conference (ACC)
San Diego, CA, USA. May 31 - June 2, 2023

On Wide-Area Control of Solar-Integrated DAE Models of Power Grids

Muhammad Nadeem — MirSaleh Bahavarnia — Ahmad F. Taha

***Abstract*— Today's power systems are controlled based on decades of experience with the fundamentals of physics-based properties of synchronous generators. Future power grids however must cope with the increasing penetration of renewable energy resources (RERs) and require a much more sophisticated control architecture. This is because RERs are formed by uncertain solar- and wind-based resources and are connected to the grid via advanced (power electronics)-based technologies. These are, in short, far more complex to control than traditional generators. RERs also do not provide inertia to damp frequency oscillations, and thus the grid's operating point changes frequently causing deterioration in the overall transient stability of the power system. This short paper proposes a robust wide-area controller for an advanced power system model having a higher order generator model, advanced (power electronics)-based solar plants model, and composite load dynamics. The simulation studies show that the proposed controller can significantly improve the transient stability of the system against uncertainty from load demand and renewables.**

***Index Terms*— Robust control, Lyapunov methods, Grid-forming inverters, Power systems, Nonlinear differential-algebraic models.**

I. Paper Introduction and Contributions

To limit frequency oscillations and to bring the power grid back to *an* equilibrium after a disturbance, three main control layers are deployed: primary, secondary, and tertiary. The primary layer usually consists of an automatic voltage regulator (AVR), power system stabilizer (PSS), generator droop control, and proportional-integral-derivative (PID) controllers—usually responsible for regulating the frequency dynamics. The secondary control layer which consists of automatic generation control (AGC) removes the steady-state error and tries to bring the system back to its nominal value, while the tertiary control layer is used for economic dispatch and redistributes the power such that the overall operating cost is minimized [1].

With the increasing penetration of renewable energy resources (RERs), the future electric grid faces major challenges, and the overall transient stability and dynamic response of the system are deteriorating [2]. For example, according to [3], [4] it has been observed in the Nordic electric network that as the penetration of RERs increases, the time the Nordic grid is spending outside the allowed frequency range (which typically ranges from $\pm$ 2–3%) is increasing significantly. This is because, unlike synchronous generators, RERs (which currently are mainly dominated by wind and solar) are intermittent, they do not provide rotational inertia, and they are connected to the grid via power electronics-based technologies. This leads to faster dynamical behavior, increased frequency nadir (the overall dip in the frequency after a large disturbance), and system oscillations.

The recent development in synchronized measurement technologies, such as phasor measurement units (PMUs), and model- and data-driven control theory encourages the development of advanced controllers that can handle the complex load demands and uncertain dynamics of renewables. For example, in [5] an $\mathcal{H}_\infty$ based load frequency controller has been proposed to handle uncertainties from tie-line power flows. In [6] a robust $\mathcal{L}_\infty$ based controller has been proposed to handle disturbances from load and renewables. In [7], [8] wide-area controllers based on PMU measurements have been proposed to damp inter-area oscillations.

Similarly, in [9] researchers have thoroughly discussed the limitations of the conventional power system control and proposed a Lyapunov stability-based controller for the nonlinear differential-algebraic equations (NDAE) model of power systems. This study does not consider renewables and load dynamics. In [10] an LMI-based decentralized controller has been proposed for frequency regulation, however, a simplified (modeling generator dynamics only) power system model has been used. Recently in [11] a two-layer (centralized for synchronous generator and decentralized for renewables) control architecture has been designed for a comprehensive power system model with solar farms, wind farms, and a higher-order generator model. The study forgoes load dynamics and modeling of algebraic equations (power flow/balance equations) in the controller synthesis.

It is notable that the majority of these studies consider a simplified representation of the power system. In the majority of the power systems control studies, renewables are usually considered as negative loads while dynamics of loads are neglected and they are commonly just modeled as constant power. That being said, we address the aforementioned limitations and propose an $\mathcal{H}_\infty$-based wide-area controller ($\mathcal{H}_\infty$ WAC) to enhance the transient stability of renewable heavy power systems. The technical contributions are as follows:

- We extended the work presented in [9], by considering an advanced interconnected power system model. The test system considered in this study models: *(i)* ninth-order synchronous machine dynamics, *(ii)* (power electronics)-based models of solar plants, *(iii)* motor loads, *(iv)*

The authors are with the Civil and Environmental Engineering Department and Taha has a joint appointment in Electrical and Computer Engineering, Vanderbilt University, 2201 West End Ave, Nashville, TN 37235, US. Emails: muhammad.nadeem@vanderbilt.edu, mirsaleh.bahavarnia@vanderbilt.edu, ahmad.taha@vanderbilt.edu. This work is supported by National Science Foundation under Grants 2152450 and 2151571.

constant power loads, and *(v)* constant impedance loads. The proposed methodology also explicitly models the algebraic equations (power flow/balance) of the power systems in the controller design.

- To handle disturbances from load and renewables, we propose an $\mathcal{H}_\infty$-based controller architecture. The static state feedback controller can be computed by solving a fairly simple LMI-based convex optimization problem. The proposed controller finds its application in wide-area monitoring and control of power systems and it improves system transient stability after a large disturbance.
- We assess the robustness of the proposed controller on the IEEE Case-9 test system which is widely used in power system control studies. The advantages of the proposed $\mathcal{H}_\infty$ WAC are also showcased by comparing the response of the power system with conventional control (primary controllers of power systems) and with $\mathcal{H}_\infty$ WAC acting on top of them.

Paper Notation: All the matrices and vectors are bold-faced. The sets are represented in calligraphic such as $\mathcal{N}, \mathcal{G}$, etc. The notation $\mathbb{R}^a$ denotes the set of column vectors with a elements. The notation $\boldsymbol{O}$ represents a zero matrix while $\boldsymbol{I}$ denotes an identity matrix of appropriate dimensions. The notation $\mathbb{R}^{a\times b}$ denotes the set of real matrices of size a-by-b. Similarly, $\mathbb{S}^{a\times b}_{++}$ denotes a positive definite matrix. The symbol $*$ represents symmetric entries in a symmetric matrix.

Note to Readers: An extended version of this short paper is available [12]. It includes further analysis, case studies, and mathematical proofs.

II. Solar and Loads-Integrated DAE Model

We consider a power system model with G synchronous generators, R solar power plants, and L_z, L_p, L_k number of constant impedance, constant power, and motor loads, respectively. The overall power system is represented as a graph $(\mathcal{N}, \mathcal{E})$, where $\mathcal{N}$ denotes the set of buses and $\mathcal{E}$ represents the set of transmission lines. Notice that $\mathcal{N} = \mathcal{G} \cup \mathcal{R} \cup \mathcal{L}$, where $\mathcal{G}$ denotes the set of buses connected to synchronous generators, $\mathcal{R}$ represents the set of buses with solar power plants, and $\mathcal{L}$ collects the set of buses connected to L_z, L_p, and L_k, respectively.

To that end, we model the solars- and loads-integrated synchronous machines-DAE (**SLS-DAE**) model of power systems using a set of differential-algebraic equations as

$$\textit{dynamic equations:} \quad \dot{\boldsymbol{x}}(t) = \boldsymbol{f}(\boldsymbol{x}_d, \boldsymbol{x}_a, \boldsymbol{u}, \boldsymbol{w}), \tag{1a}$$

$$\textit{algebraic equations:} \quad \boldsymbol{0} = \boldsymbol{h}(\boldsymbol{x}_d, \boldsymbol{x}_a, \boldsymbol{u}, \boldsymbol{w}), \tag{1b}$$

where $\boldsymbol{x}_d \in \mathbb{R}^{n_d}$ represents the dynamic variables, $\boldsymbol{x}_a \in \mathbb{R}^{n_a}$ represents algebraic variables of the power network, $\boldsymbol{u} \in \mathbb{R}^{n_u}$ models the control inputs, and $\boldsymbol{w} \in \mathbb{R}^{n_w}$ denotes exogenous disturbances.

In (1), vector $\boldsymbol{x}_a$ is modeled as

$$\boldsymbol{x}_a := \boldsymbol{x}_a(t) = \begin{bmatrix} \boldsymbol{I}_{\mathrm{Re}}^\top & \boldsymbol{I}_{\mathrm{Im}}^\top & \boldsymbol{V}_{\mathrm{Re}}^\top & \boldsymbol{V}_{\mathrm{Im}}^\top \end{bmatrix}^\top \in \mathbb{R}^{n_a}, \tag{2}$$

where $\boldsymbol{I}_{\mathrm{Re}} = \{I_{\mathrm{Re}_i}\}_{i\in\mathcal{N}}, \boldsymbol{I}_{\mathrm{Im}} = \{I_{\mathrm{Im}_i}\}_{i\in\mathcal{N}}, \boldsymbol{V}_{\mathrm{Re}} = \{V_{\mathrm{Re}_i}\}_{i\in\mathcal{N}}, \boldsymbol{V}_{\mathrm{Im}} = \{V_{\mathrm{Im}_i}\}_{i\in\mathcal{N}}$ represent the real and imaginary parts of currents and voltages, respectively. The vector $\boldsymbol{u}$ models the control inputs of synchronous generators and solar PV plants and is represented as

$$\boldsymbol{u} := \boldsymbol{u}(t) = \begin{bmatrix} \boldsymbol{u}_G^\top & \boldsymbol{u}_R^\top \end{bmatrix}^\top \in \mathbb{R}^{n_u}, \tag{3}$$

where $\boldsymbol{u}_G = \begin{bmatrix} \boldsymbol{V}_{\mathrm{ref}}^\top & \boldsymbol{P}_{v_{\mathrm{ref}}}^\top \end{bmatrix}^\top \in \mathbb{R}^{2G}$ with $\boldsymbol{V}_{\mathrm{ref}}$ and $\boldsymbol{P}_{v_{\mathrm{ref}}}$ denoting reference set-points for voltages (pu) and turbine valve positions (pu) of the synchronous generator, respectively. Similarly, $\boldsymbol{u}_R = \begin{bmatrix} \boldsymbol{V}_{\mathrm{ref}}^\top & \boldsymbol{P}_{\mathrm{ref}}^\top \end{bmatrix}^\top \in \mathbb{R}^{2R}$, where $\boldsymbol{P}_{\mathrm{ref}}$ and $\boldsymbol{V}_{\mathrm{ref}}$ are the power (pu) and voltage (pu) reference set points for solar PV plants. Also, we define $\boldsymbol{w}$ in Eq. (1) as $\boldsymbol{w} = \begin{bmatrix} \boldsymbol{I}_r^\top & \boldsymbol{P}_d^\top \end{bmatrix}^\top \in \mathbb{R}^{n_w}$ where $\boldsymbol{I}_r$ is the solar irradiance (W/m^2) on the PV plants and $\boldsymbol{P}_d$ is the system real power load demand (pu).

Moreover, in Eq. (1), we represent $\boldsymbol{x}_d$ as

$$\boldsymbol{x}_d := \boldsymbol{x}_d(t) = \begin{bmatrix} \boldsymbol{x}_G^\top & \boldsymbol{x}_R^\top & \boldsymbol{x}_m^\top \end{bmatrix}^\top \in \mathbb{R}^{n_d}, \tag{4}$$

where $\boldsymbol{x}_G$ are the dynamic states of the conventional power plant (states of synchronous generator, excitation system, governor, and turbine dynamics), $\boldsymbol{x}_R$ represents the differential states of the solar power plant, and $\boldsymbol{x}_m$ denotes the states of motor loads. With that in mind, we model the conventional power plant via a comprehensive 9^{th}-order model, and thus vector $\boldsymbol{x}_G$ can be expressed as follows [13], [14]:

$$\boldsymbol{x}_G = \begin{bmatrix} \boldsymbol{\delta}_{sg}^\top & \boldsymbol{\omega}_{sg}^\top & \boldsymbol{e}_q^\top & \boldsymbol{e}_d^\top & \boldsymbol{P}_v^\top & \boldsymbol{T}_m^\top & \boldsymbol{E}_{fd}^\top & \boldsymbol{v}_a^\top & \boldsymbol{r}_f^\top \end{bmatrix}^\top \in \mathbb{R}^{9G}, \tag{5}$$

where $\boldsymbol{\delta}_{sg}$ denotes generator rotor angle (pu), $\boldsymbol{\omega}_{sg}$ is the generator speed (pu), $\boldsymbol{e}_q$, $\boldsymbol{e}_d$, represent transient voltages along dq-axis (pu), $\boldsymbol{P}_v$ is the turbine valve position (pu), $\boldsymbol{T}_m$ denotes turbines prime mover torque (pu), $\boldsymbol{E}_{fd}$ is the generator field voltage (pu), $\boldsymbol{r}_f$ denotes stabilizer output (pu), and $\boldsymbol{v}_a$ represents amplifier voltage (pu) [13], [14]. The dynamic model for the solar power plant is taken from [15], which models solar farms in *grid-forming* mode, and thus vector $\boldsymbol{x}_R$ can be written as

$$\boldsymbol{x}_R = \begin{bmatrix} \boldsymbol{\delta}_{\mathrm{inv}}^\top & \boldsymbol{v}_{dq_c}^\top & \boldsymbol{i}_{dqf}^\top & \boldsymbol{P}_e^\top & \boldsymbol{Q}_e^\top & \boldsymbol{E}_{dc}^\top & \boldsymbol{z}_{dqf}^\top & \boldsymbol{z}_{dq0}^\top \end{bmatrix}^\top \in \mathbb{R}^{12R}, \tag{6}$$

where $\boldsymbol{\delta}_{\mathrm{inv}}$ represents the inverter angle (pu) of solar power plants, $\boldsymbol{v}_{dq_c} = [\boldsymbol{v}_{d_c}^\top \ \boldsymbol{v}_{q_c}^\top]$ are the voltages (pu) across the AC capacitor along dq-axis, $\boldsymbol{i}_{dq_f} = [\boldsymbol{i}_{d_f}^\top \ \boldsymbol{i}_{q_f}^\top]$ represent the currents (pu) at the terminals of the inverter along dq-axis, $\boldsymbol{P}_e$, $\boldsymbol{Q}_e$ are the total real and reactive power injected by $S1$ and $S2$ to the grid, $\boldsymbol{E}_{\mathrm{dc}}$ is the energy stored in the DC side capacitor, and $\boldsymbol{z}_{dqf} = [\boldsymbol{z}_{d_f}^\top \ \boldsymbol{z}_{q_f}^\top]$, $\boldsymbol{z}_{dq_o} = [\boldsymbol{z}_{d_0}^\top \ \boldsymbol{z}_{q_0}^\top]$ are the dynamic states of the current and voltage regulator of $S1$ and $S2$. Notice that from E_{dc} the DC-link voltage V_{dc} can also be computed as $V_{dc} = \sqrt{E_{dc}}$. To obtain further information and a detailed description of the solar power plant model used in this study, readers are referred to [15].

In (4), the model for the motor loads is defined as [16]:

$$\dot{\omega}_{\mathrm{mot}} = \frac{1}{2H_m}(T_e - T_m), \tag{7}$$

where T_m, T_e are the mechanical and electromagnetic torques, respectively, ω_{mot} is the motor speed, and H_m is the motor inertia constant [16, p. 244]. Thus, vector $\boldsymbol{x}_m$ only has one state $[\boldsymbol{\omega}_{\mathrm{mot}}]$. This completes the modeling of system dynamics

(1a). Now, the model for the algebraic constraints Eq. (1b) is expressed as [13]

$$\underbrace{\begin{bmatrix}\widetilde{\boldsymbol{I}}_G\\ \widetilde{\boldsymbol{I}}_R\\ \widetilde{\boldsymbol{I}}_L\end{bmatrix}}_{\boldsymbol{I}} - \underbrace{\begin{bmatrix}\boldsymbol{Y}_{GG} & \boldsymbol{Y}_{GR} & \boldsymbol{Y}_{GL}\\ \boldsymbol{Y}_{RG} & \boldsymbol{Y}_{RR} & \boldsymbol{Y}_{RL}\\ \boldsymbol{Y}_{LG} & \boldsymbol{Y}_{LR} & \boldsymbol{Y}_{LL}\end{bmatrix}}_{\boldsymbol{Y}} \underbrace{\begin{bmatrix}\widetilde{\boldsymbol{V}}_G\\ \widetilde{\boldsymbol{V}}_R\\ \widetilde{\boldsymbol{V}}_L\end{bmatrix}}_{\boldsymbol{V}} = \boldsymbol{0}, \tag{8}$$

where matrix $\boldsymbol{Y} \in \mathbb{R}^{N\times N}$ represents the system admittance matrix, vector $\boldsymbol{I}$ denotes the net current, and vector $\boldsymbol{V}$ lumps all the bus voltages. Note that Eq. (8) describes the overall current balance equation between the generation and demand sides. In (8), vector $\widetilde{\boldsymbol{V}}_G = \{V_{Re_i}\}_{i\in\mathcal{G}} + j\{V_{Im_i}\}_{i\in\mathcal{G}}$ encapsulates all the voltage phasors at the terminal buses of synchronous machines and $\widetilde{\boldsymbol{I}}_G = \{I_{Re_i}\}_{i\in\mathcal{G}} + j\{I_{Im_i}\}_{i\in\mathcal{G}}$ lumps all the phasor currents supplied by synchronous machines. Similarly, vectors $\widetilde{\boldsymbol{I}}_R$, $\widetilde{\boldsymbol{I}}_L$, and $\widetilde{\boldsymbol{V}}_R$, $\widetilde{\boldsymbol{V}}_L$ collect current and voltage phasors at buses connected with $S1$, $S2$, and loads, respectively.

That being said, by considering equations (2)–(8) and including the associated dynamic and algebraic models given in [13], [15], we can express the overall SLS-DAE model of power systems in a descriptor state-space format as follows:

$$\textbf{SLS-DAE:}\quad \boldsymbol{E}\dot{\boldsymbol{x}} = \boldsymbol{A}\boldsymbol{x} + \boldsymbol{f}\left(\boldsymbol{x},\boldsymbol{u},\boldsymbol{w}\right) + \boldsymbol{B}_u\boldsymbol{u} + \boldsymbol{B}_w\boldsymbol{w}, \tag{9}$$

where $\boldsymbol{x} = \begin{bmatrix}\boldsymbol{x}_d^\top & \boldsymbol{x}_a^\top\end{bmatrix}^\top \in \mathbb{R}^{n_x}$ is the state vector and $\boldsymbol{E} \in \mathbb{R}^{n_x\times n_x}$ is a singular matrix encoding algebraic constraints with rows of zeros, while the constant system matrices $\boldsymbol{A} \in \mathbb{R}^{n_x\times n_x}$, $\boldsymbol{B} \in \mathbb{R}^{n_x\times n_u}$, $\boldsymbol{B}_w \in \mathbb{R}^{n_x\times n_w}$ have been obtained by capturing the linear component of (1) and the function $\boldsymbol{f}(\cdot) \in \mathbb{R}^{n_x}\times\mathbb{R}^{n_u}\times\mathbb{R}^{n_w} \to \mathbb{R}^{n_f}$ represents the associated nonlinearities in the system model.

III. Robust Wide-Area Controller for SLS-DAE

In this section, we present the architecture of the proposed $\mathcal{H}_\infty$ WAC for the SLS-DAE model of power systems (9). The primary objective of the formulation is to design a control law that provides additional control inputs to both synchronous generators and solar power plants in the presence of large unknown disturbances from load demand and renewables. The main objective of the proposed controller is to damp out oscillations and quickly restore system frequency to its nominal value after large unknown disturbances in load demand and renewable generation.

The SLS-DAE model of power systems (9) with the proposed $\mathcal{H}_\infty$ WAC is expressed as

$$\boldsymbol{E}\dot{\boldsymbol{x}} = \boldsymbol{A}\boldsymbol{x} + \boldsymbol{f}\left(\boldsymbol{x},\boldsymbol{u}_{\text{wac}},\boldsymbol{w}\right) + \boldsymbol{B}\boldsymbol{u}_{\text{wac}} + \boldsymbol{B}_w\boldsymbol{w}, \tag{10}$$

where for $kT \le t < (k+1)T$ the controller law $\boldsymbol{u}_{\text{wac}}$ is designed as follows:

$$\boldsymbol{u}_{\text{wac}} := \boldsymbol{u}_{\text{wac}}(t) = \boldsymbol{u}_{ref}^k + \boldsymbol{K}\left(\boldsymbol{x}(t) - \boldsymbol{x}^k(t)\right). \tag{11}$$

In the control law (11), $\boldsymbol{u}_{ref}^k$ is the reference or baseline control inputs for the synchronous machines and renewables which are usually determined for every k^{th}-dispatch time-period using power flow studies. For a given load demand and renewable generation, the control signal $\boldsymbol{u}_{ref}^k$ keeps the SLS-DAE system (9) at a particular steady-state $\boldsymbol{x}^k(t)$. The matrix $\boldsymbol{K} \in \mathbb{R}^{n_u\times n_x}$ is the static state feedback matrix for the controller and it is determined with the help of the knowledge of constant matrices ($\boldsymbol{A}$, $\boldsymbol{B}_u$, and $\boldsymbol{B}_w$) in SLS-DAE model (9). Further discussion on the computation of matrix $\boldsymbol{K}$ is given later in this section. The overall architecture of the proposed $\mathcal{H}_\infty$ WAC is presented in Fig. 1. We observe from Fig. 1 that the overall control law requires the knowledge of both differential and algebraic states of the system. This requirement can easily be satisfied since the plethora of dynamic state estimator (DSE) algorithms exists in the literature—see [17]–[19] that can provide very accurate estimates of all the states of the power systems using PMU measurements.

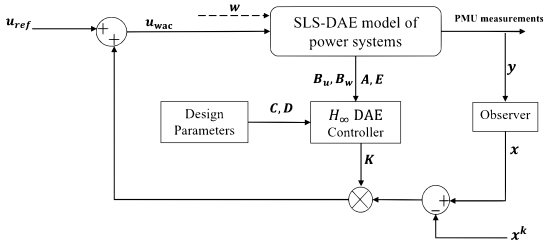

Fig. 1. Architecture of the proposed $\mathcal{H}_\infty$ WAC. Vector $\boldsymbol{x}$ is the overall state vector, $\boldsymbol{w}$ encapsulates the total load demand of the system and irradiance of the solar plants, while $\boldsymbol{y}$ contains the measurements received from PMUs sensors.

To proceed with the computation of controller matrix $\boldsymbol{K}$, let us assume $\boldsymbol{w}^s$ and $\boldsymbol{x}^s$ be the post-fault steady-state values of the SLS-DAE model (9). Then, the system dynamics (9) with the proposed controller at this new equilibrium point can be written as

$$\boldsymbol{0} = \boldsymbol{A}\boldsymbol{x}^s + \boldsymbol{f}\left(\boldsymbol{x}^s,\boldsymbol{u}_{\text{wac}},\boldsymbol{w}^s\right) + \boldsymbol{B}_u(\boldsymbol{u}_{ref}^k + \boldsymbol{K}(\boldsymbol{x}^s - \boldsymbol{x}^k)) + \boldsymbol{B}_w\boldsymbol{w}^s.$$

Now, to examine the system dynamic behavior before and after the occurrence of any fault/disturbances, let us introduce new variables $\bar{\boldsymbol{x}}_a = \boldsymbol{x}_a - \boldsymbol{x}_a^s \in \mathbb{R}^{n_a}$, $\bar{\boldsymbol{x}}_d = \boldsymbol{x}_d - \boldsymbol{x}_d^s \in \mathbb{R}^{n_d}$, and $\bar{\boldsymbol{w}} = \boldsymbol{w} - \boldsymbol{w}^s \in \mathbb{R}^{n_w}$. These new variables describe the deviations of algebraic and dynamic states of the perturbed SLS-DAE model around the post-fault system steady-state values $\boldsymbol{x}^s$ and $\boldsymbol{w}^s$. With that in mind, the perturbed closed-loop SLS-DAE model of power systems can be expressed as follows:

$$\boldsymbol{E}\dot{\bar{\boldsymbol{x}}} = (\boldsymbol{A} + \boldsymbol{B}_u\boldsymbol{K})\bar{\boldsymbol{x}} + \bar{\boldsymbol{f}}(\bar{\boldsymbol{x}},\boldsymbol{u}_{\text{wac}},\bar{\boldsymbol{w}}) + \boldsymbol{B}_w\bar{\boldsymbol{w}}, \tag{12}$$

where $\bar{\boldsymbol{f}}(\bar{\boldsymbol{x}},\boldsymbol{u}_{\text{wac}},\bar{\boldsymbol{w}}) = \boldsymbol{f}(\boldsymbol{x},\boldsymbol{u}_{\text{wac}},\boldsymbol{w}) - \boldsymbol{f}(\boldsymbol{x}^s,\boldsymbol{u}_{\text{wac}},\boldsymbol{w}^s)$.

Note that $\bar{\boldsymbol{w}}$ denotes the deviation of system total load demand and solar irradiance from their respective post-fault equilibrium $\boldsymbol{w}^s$. Our main objective herein is to compute controller matrix $\boldsymbol{K}$ in a way such that the solution trajectories of the perturbed SLS-DAE model (12) asymptotically converge to zero under unknown disturbances caused by $\bar{\boldsymbol{w}}$ (which describes the mismatch between generation and demand and disturbances in solar power caused by uncertainties in solar irradiance).

In the following section, we present the theory of our proposed $\mathcal{H}_\infty$ WAC which is primarily based on Lyapunov stability, and the $\mathcal{H}_\infty$ notion is used for achieving robust performance under unknown disturbances from load demand and renewable generation.

$\mathcal{H}_\infty$ Notion and WAC Design: To synthesize robust controllers, $\mathcal{H}_\infty$-based control designs are the most powerful and well-established tools in modern control theory literature. The core idea in $\mathcal{H}_\infty$-based control is that first, a performance criterion/index is established, and then, the controller matrix is designed in a way such that using state/output feedback, the controller ensures the minimum impact of unknown disturbances on the designed performance criterion [20].

That being said, let us define $\boldsymbol{z} := \boldsymbol{z}(t) = \boldsymbol{C}\boldsymbol{x}(t) + \boldsymbol{D}\boldsymbol{u}_{\text{wac}}(t) \in \mathbb{R}^{n_x}$ to be the performance criterion for the control law $\boldsymbol{u}_{\text{wac}}$, where $\boldsymbol{C} \in \mathbb{R}^{n_x \times n_x}$ and $\boldsymbol{D} \in \mathbb{R}^{n_x \times n_u}$ are constant known matrices. Similar to the penalizing matrices $\boldsymbol{Q}$ and $\boldsymbol{R}$ in the conventional linear-quadratic regulator (LQR), matrices $\boldsymbol{C}$ and $\boldsymbol{D}$ can be selected based on the electrical grid operator preferences, meaning how much and which state or control input needs to be penalized while determining the controller matrix $\boldsymbol{K}$. Likewise, the previous derivation, the perturbed performance criterion around post-fault equilibrium $\boldsymbol{x}^s$ can be expressed as $\bar{\boldsymbol{z}} = \boldsymbol{z} - \boldsymbol{z}^s = (\boldsymbol{C} + \boldsymbol{D}\boldsymbol{K})\bar{\boldsymbol{x}}$. Then, the perturbed SLS-DAE model (12) with the performance index $\bar{\boldsymbol{z}}$ can be written as follows:

$$\boldsymbol{E}\dot{\bar{\boldsymbol{x}}} = (\boldsymbol{A} + \boldsymbol{B}_u\boldsymbol{K})\bar{\boldsymbol{x}} + \bar{\boldsymbol{f}}(\bar{\boldsymbol{x}}, \boldsymbol{u}_{\text{wac}}, \bar{\boldsymbol{w}}) + \boldsymbol{B}_w\bar{\boldsymbol{w}}, \tag{13a}$$

$$\bar{\boldsymbol{z}} = (\boldsymbol{C} + \boldsymbol{D}\boldsymbol{K})\bar{\boldsymbol{x}}. \tag{13b}$$

Then, the system (13) is $\mathcal{H}_\infty$ stable, if for any bounded uncertainty/disturbance in load demand and renewable generation, the magnitude of the performance criterion $\bar{\boldsymbol{z}}$ always remains less then constant times the magnitude of uncertainty $\bar{\boldsymbol{w}}$, i.e., $\|\bar{\boldsymbol{z}}\|_{L_2}^2 < \mu^2\|\bar{\boldsymbol{w}}\|_{L_2}^2$ [21].

To that end, we now pose the computation of controller matrix $\boldsymbol{K}$ as a convex semi-definite program (SDP) which guarantees that the SLS-DAE model of power system (13) is always $\mathcal{H}_\infty$ stable against unknown disturbances from load and renewable generation as follows:

$$\begin{aligned} (\mathbf{OP}) \quad \underset{\boldsymbol{H},\boldsymbol{X},\boldsymbol{W},\lambda,\kappa_1,\kappa_2}{\text{minimize}} \quad & a_1\lambda + a_2\kappa_1 + a_3\kappa_2 \\ \text{subject to} \quad & \text{LMI (14)},\ \text{LMIs (15)},\ \boldsymbol{X} \succ 0, \\ & \lambda > 0,\ \kappa_1 > 0,\ \kappa_2 > 0, \end{aligned}$$

where

- a_1, a_2, and a_3 are predefined weighting constants.
- The variables in **OP** are real-valued matrices $\boldsymbol{H} \in \mathbb{R}^{n_u \times n_x}$, $\boldsymbol{W} \in \mathbb{R}^{n_a \times n_x}$, positive-definite matrix $\boldsymbol{X} \in \mathbb{S}_{++}^{n_x \times n_x}$, and positive scalars $\lambda, \kappa_1, \kappa_2 \in \mathbb{R}_{++}$.
- LMI (14) is defined as

$$\begin{bmatrix} \boldsymbol{\Psi} & * & * \\ \boldsymbol{B}_w^\top & -\lambda\boldsymbol{I} & * \\ \boldsymbol{C}(\boldsymbol{X}\boldsymbol{E}^\top + \boldsymbol{E}^\perp\boldsymbol{W}) + \boldsymbol{D}\boldsymbol{H} & \boldsymbol{O} & -\boldsymbol{I} \end{bmatrix} \prec 0, \tag{14}$$

  with $\boldsymbol{\Psi}$ given as

$$\boldsymbol{\Psi} = (\boldsymbol{X}\boldsymbol{E}^\top + \boldsymbol{E}^\perp\boldsymbol{W})^\top\boldsymbol{A}^\top + \boldsymbol{A}(\boldsymbol{X}\boldsymbol{E}^\top + \boldsymbol{E}^\perp\boldsymbol{W}) + \boldsymbol{H}^\top\boldsymbol{B}^\top + \boldsymbol{B}\boldsymbol{H},$$

  where $\boldsymbol{E}^\perp \in \mathbb{R}^{n_x \times n_a}$ is the orthogonal complement of $\boldsymbol{E}$.

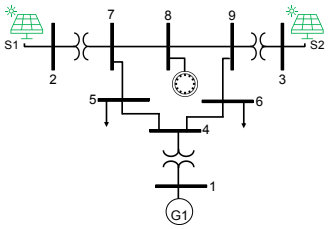

Fig. 2. One line diagram of the modified WECC test power system with a motor load at Bus 8, a synchronous generator at Bus 1, and two solar power plants $S1$ and $S2$ at Buses 2 and 3.

- LMIs (15) are defined as:

$$\begin{bmatrix} -\kappa_1\boldsymbol{I} & \boldsymbol{H}^\top \\ \boldsymbol{H} & -\boldsymbol{I} \end{bmatrix} \prec 0, \quad \begin{bmatrix} -\kappa_2\boldsymbol{I} & \boldsymbol{I} \\ \boldsymbol{I} & -\boldsymbol{S} - \boldsymbol{S}^\top \end{bmatrix} \prec 0, \tag{15}$$

  with $\boldsymbol{S} = \boldsymbol{X}\boldsymbol{E}^\top + \boldsymbol{E}^\perp\boldsymbol{W}$.
- Controller matrix $\boldsymbol{K}$ can be retrieved as

$$\boldsymbol{K} = \boldsymbol{H}(\boldsymbol{X}\boldsymbol{E}^\top + \boldsymbol{E}^\perp\boldsymbol{W})^{-1}.$$

- **OP** is a convex semi-definite problem and can be easily solved via various convex optimization toolboxes.

For brevity, the motivation and proof behind **OP** are omitted and included in the extended manuscript [12]. Calculating controller matrix $\boldsymbol{K}$ by solving **OP** always ensures that after a large mismatch between generation and demand, the perturbed SLS-DAE (13) remains $\mathcal{H}_\infty$ stable, such that $\|\bar{\boldsymbol{z}}\|_{L_2}^2 < \mu^2\|\bar{\boldsymbol{w}}\|_{L_2}^2$, where $\lambda = \mu^2$ in LMI (14). Thus, the designed control law (11) tries to minimize the impact of unknown disturbances on the system dynamics. By doing so, in the below numerical case studies section, we show that the proposed $\mathcal{H}_\infty$ WAC decreases system oscillations and frequency nadir, and quickly restores the SLS-DAE model nominal frequency after any fault/disturbance.

IV. Simulation Studies

The proposed wide-area controller has been tested on a modified WECC (Western electricity coordinate council) power system [1], which is a simplified representation of North American Western interconnection. This test system consists of a total of 9 buses, one synchronous generator $G1$ connected at Bus 1, constant power and constant impedance load at both Buses 5 and 6, an induction motor load connected at Bus 8, and two solar power plants $S1$ and $S2$ at Buses 2 and 3. The single-line diagram of this test system is shown in Fig. 2. All the parameters (for synchronous generators, solar plants, and loads) and a further detailed explanation of the dynamics of the test power system used in this study can be found in [13], [15]

The numerical simulations are carried out on a personal computer having 64GB of RAM and a 16-core Intel $i9 - 11980HK$ processor. All the case studies are implemented in MATLAB $R2021a$. The SLS-DAE model (10) is solved via MATLAB's differential-algebraic system solver `ode15s`. The settings for the `ode15s` are selected to be: (i) absolute tolerance $= 10^{-6}$, (ii) maximum step size $= 10^{-4}$, and (iii) relative tolerance $= 10^{-6}$. The system bases are considered to be $S_b = 100\text{MVA}$ and $w_b = 120\pi\text{rad/s}$. The SDP

optimization problem **OP** is modeled in YALMIP [22] and is solved via a MOSEK solver [23]. The initial steady-state values for the power system before the occurrence of any disturbances are computed using power flow solutions through `runpf` function in MATPOWER [24]. Furthermore, for all the case studies, it has been assumed that an observer/estimator is already present in the system and is estimating all the states of the power system in real-time which are then fed as state feedback to the $\mathcal{H}_\infty$ WAC as depicted in Fig. 1.

A. Case A: Performance Under Load Disturbances

In this section, we assess the performance of the proposed WAC in the presence of large disturbances in the overall load demand of the power network. To that end, the simulation studies for this section are carried out as follows: Initially, the system operates in equilibrium conditions (meaning total power generation is equal to the total load demand $P_d^0 + Q_d^0 = 0.77 + j0.25$ pu). Thus, there are no transients in the system states, and all the dynamic and algebraic states rest at their steady-state values. Then, right after $t > 0$ the total load demand of the SLS-DAE model has abruptly been increased to a new value given as $P_d^s + Q_d^s = (1 + \delta_d)(P_d^0 + Q_d^0)$, where δ_d specifies the severity of the disturbance and here, it is chosen to be $\delta_d = 0.5$. This disturbance will eventually throw the power system to a new equilibrium or maybe make it unstable. The objective of the controller is to dampen the system oscillations and restore system frequency as soon as possible to its nominal value.

The results for this case study are shown in Fig. 3. To advocate the advantages of the proposed $\mathcal{H}_\infty$ WAC, a comparison between the system dynamics response after a disturbance with only conventional control and with the proposed $\mathcal{H}_\infty$ WAC on top of it has also been carried out. The conventional control is comprised of the legacy control devices used in the power systems—that are, governor, PSS, and AVR for the synchronous generators [13] and proportional-integral (PI) and droop controllers for the solar power plants [15], [25].

From Fig. 3, we clearly observe that with the proposed $\mathcal{H}_\infty$ WAC, the system oscillations during the transient period (first few seconds of simulations) have significantly been damped out. Also, the frequency nadir is significantly improved, with just conventional control the overall dip in the frequency is 0.9843 (pu) while with proposed WAC, it improved to 0.996 (pu).

Notice that the inverter angular speed $\boldsymbol{\omega}_{\text{inv}}$ and slip $\boldsymbol{s}_{\text{inv}}$ have been computed from the state vectors as follows:

$$\boldsymbol{\omega}_{\text{inv}} = 1 - k_{\text{inv}}(\tilde{\boldsymbol{P}}_e - \boldsymbol{P}_{\text{ref}}), \boldsymbol{s}_{\text{inv}} = (w_e - \boldsymbol{\omega}_{\text{inv}})/w_e,$$

where k_{inv} is the inverter droop constant and w_e is the overall weighted-average system frequency.

To further advocate the advantages of the proposed controller, we add further disturbance in the system, this time by decreasing the load demand of the SLS-DAE model such that $P_d^s + Q_d^s = (1 - \delta_d)(P_d^0 + Q_d^0)$ where $\delta_d = 0.5$. The results are presented in Fig. 4. We observe that the controller is still significantly increasing the overall transient stability of the system by adding damping to the oscillations and driving the system back to its equilibrium values.

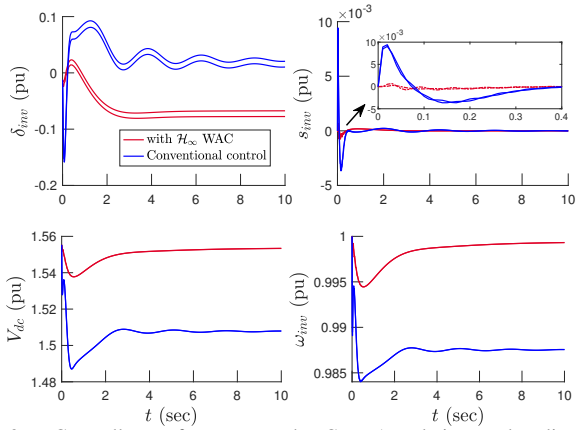

Fig. 3. Controller performance under Case A: relative angle, slip, DC-link voltage, and angular speed of both solar plants $S1$ and $S2$ with only conventional control and with $\mathcal{H}_\infty$ WAC acting on top of them.

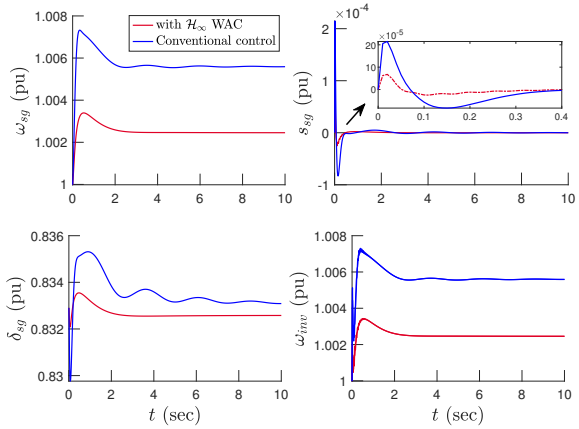

Fig. 4. Controller performance under sudden decrease in load demand: $G1$ rotor speed, $G1$ slip, $G1$ rotor angle, and angular speed of both solar plants $S1$ and $S2$.

Moreover, we also observe from Figs. 3 and 4 that after a large disturbance, with the proposed $\mathcal{H}_\infty$ WAC, the system frequency is almost restored to its nominal value while with only conventional control, the system frequency settles to a value below its nominal value. This also indicates that with the proposed $\mathcal{H}_\infty$ WAC, the work required by well-known AGC (which mainly works as a PI-type controller and is primarily responsible to remove the steady-state error in the frequency and restore it to its nominal value) in the power systems is reduced.

B. Case B: Performance in the Presence of Uncertainty in Solar Irradiance and Load Demand

Here, we evaluate the robustness of the proposed controller in the presence of uncertainty in both load demand and the sun's irradiance on the solar power plants. Similar to as done in the previous case study, right after the start of the simulation, the irradiance I_r on both $S1$ and $S2$ has suddenly decreased by 30% as $I_r^d = (1 + \delta_I)(I_r^0)$, with $\delta_I = 0.3$, where I_r^0 and I_r^d are the sun's irradiance before and after the disturbance, respectively. The load demand is increased as $P_d^s + Q_d^s = (1 + \delta_d)(P_d^0 + Q_d^0)$ with δ_d chosen this time to be $\delta_d = 0.9$. The results are shown in Fig. 5. We observe that the conventional/primary controllers of the SLS-DAE model are

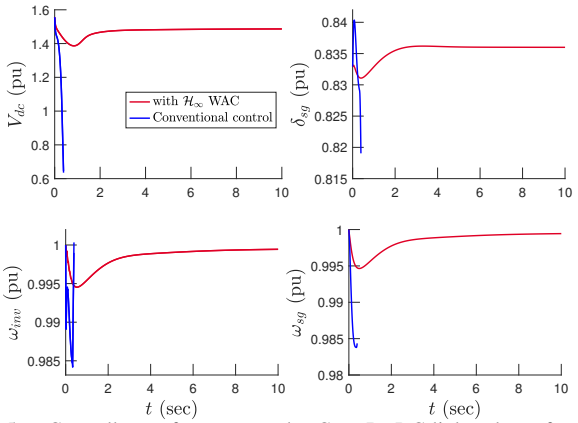

Fig. 5. Controller performance under Case B: DC-link voltage for both $S1$ and $S2$, $G1$ rotor angle, angular speed of $S1$ and $S2$, and $G1$ rotor speed.

unable to control the system and the power network becomes unstable and loses its synchronicity. While with $\mathcal{H}_\infty$ WAC acting on top of it and sending additional control signal $\boldsymbol{u}_{\text{wac}}$ to these primary controllers, the power system remains stable and synchronized. Furthermore, from Fig. 5 we also verify that the proposed controller not only keeps the SLS-DAE model stable but also recovers the system to its nominal value. Further case studies on a larger system are included in [12].

V. Conclusions and Future Work

In this paper, we propose a new robust state feedback controller for power systems namely $\mathcal{H}_\infty$ WAC. The presented controller is applied to an advanced interconnected power system model. The proposed controller is robust against uncertainties from load demands and renewables and can significantly improve the overall transient stability of the power system after a large disturbance. The presented controller is highly feasible for practical applications as it sends additional control signals to the already present primary controllers of the power system and does not require any new installation of control equipment.

The limitations of the study are twofold: Firstly, the presented controller structure is dense and not sparse, Second, the proposed controller may not be robust to changes in system matrices unless these changes are specifically modeled in controller design. Future work will be about addressing the aforementioned issues in the proposed controller design.

References

[1] P. Anderson and A. Fouad, *Power System Control and Stability (IEEE Press Power Engineering Series)*, ser. 2nd edition Wiley. Wiley, 2003.

[2] N. H. et al, "Definition and classification of power system stability – revisited extended," *IEEE Transactions on Power Systems*, vol. 36, no. 4, pp. 3271–3281, 2021.

[3] A. M. Ersdal, D. Fabozzi, L. Imsland, and N. F. Thornhill, "Model predictive control for power system frequency control taking into account imbalance uncertainty," *IFAC Proceedings Volumes*, vol. 47, no. 3, pp. 981–986, 2014, 19th IFAC World Congress. [Online]. Available: https://www.sciencedirect.com/science/article/pii/S1474667016417428

[4] A. M. Ersdal, L. Imsland, and K. Uhlen, "Model predictive load-frequency control," *IEEE Transactions on Power Systems*, vol. 31, no. 1, pp. 777–785, 2016.

[5] N. Chuang, "Robust $\mathcal{H}_\infty$ load frequency control in interconnected power systems," in *Australasian Universities Power Engineering Conference (AUPEC)*, 2013, pp. 1–6.

[6] A. F. Taha, M. Bazrafshan, S. A. Nugroho, N. Gatsis, and J. Qi, "Robust control for renewable-integrated power networks considering input bound constraints and worst case uncertainty measure," *IEEE Transactions on Control of Network Systems*, vol. 6, no. 3, pp. 1210–1222, 2019.

[7] F. Dorfler, M. R. Jovanović, M. Chertkov, and F. Bullo, "Sparsity-promoting optimal wide-area control of power networks," *IEEE Transactions on Power Systems*, vol. 29, no. 5, pp. 2281–2291, 2014.

[8] S. Zhang and V. Vittal, "Design of wide-area power system damping controllers resilient to communication failures," *IEEE Transactions on Power Systems*, vol. 28, no. 4, pp. 4292–4300, 2013.

[9] S. A. Nugroho and A. F. Taha, "How vintage linear systems controllers have become inadequate in renewables-heavy power systems: Limitations and new solutions," in *American Control Conference (ACC)*, 2022, pp. 4553–4558.

[10] L. D. Marinovici, J. Lian, K. Kalsi, P. Du, and M. Elizondo, "Distributed hierarchical control architecture for transient dynamics improvement in power systems," *IEEE Transactions on Power Systems*, vol. 28, no. 3, pp. 3065–3074, 2013.

[11] T. Sadamoto, A. Chakrabortty, T. Ishizaki, and J.-i. Imura, "Dynamic modeling, stability, and control of power systems with distributed energy resources: Handling faults using two control methods in tandem," *IEEE Control Systems Magazine*, vol. 39, no. 2, pp. 34–65, 2019.

[12] M. Nadeem, M. Bahavarnia, and A. F. Taha. (2023) Robust feedback control of power systems with grid-forming solar plants and composite loads. In review. Links: https://www.dropbox.com/s/be6n5wluoxog2r7/SLSDAEControl.pdf?dl=0 or https://bit.ly/3mRS8Vi.

[13] P. Sauer, M. Pai, and J. Chow, *Power System Dynamics and Stability: With Synchrophasor Measurement and Power System Toolbox*, ser. Wiley - IEEE. Wiley, 2017.

[14] H. N. V. Pico and B. B. Johnson, "Transient stability assessment of multi-machine multi-converter power systems," *IEEE Transactions on Power Systems*, vol. 34, no. 5, pp. 3504–3514, 2019.

[15] S. Roy and H. N. V. Pico, "Transient stability and active protection of power systems with grid-forming pv power plants," *IEEE Transactions on Power Systems*, vol. 38, no. 1, pp. 897–911, 2022.

[16] P. C. Krause, O. Wasynczuk, S. D. Sudhoff, and S. D. Pekarek, *Analysis of Electric Machinery and Drive Systems*, 3rd ed. John Wiley & Sons, 2013.

[17] M. Nadeem, S. A. Nugroho, and A. F. Taha, "Dynamic state estimation of nonlinear differential algebraic equation models of power networks," *IEEE Transactions on Power Systems*, pp. 1–14, 2022.

[18] M. Nadeem and A. F. Taha, "Robust dynamic state estimation of multi-machine power networks with solar farms and dynamics loads," in *2022 IEEE 61st Conference on Decision and Control (CDC)*, 2022, pp. 7174–7179.

[19] M. Nadeem, A. F. Taha, and S. A. Nugroho, "Impact of uncertainty from renewables on dynamic state estimation of power networks," in *2022 IEEE Power and Energy Society General Meeting (PESGM)*, 2022, pp. 1–5.

[20] Q. Lam, A. Bratcu, and D. Riu, "Robustness analysis of primary frequency $\mathcal{H}_\infty$ control in stand-alone microgrids with storage units," *IFAC-PapersOnLine*, vol. 49, no. 27, pp. 123–128, 2016, iFAC Workshop on Control of Transmission and Distribution Smart Grids CTDSG. [Online]. Available: https://www.sciencedirect.com/science/article/pii/S2405896316323497

[21] A. D. Rosaline and U. Somarajan, "Structured h-infinity controller for an uncertain deregulated power system," *IEEE Transactions on Industry Applications*, vol. 55, no. 1, pp. 892–906, 2019.

[22] J. Lofberg, "Yalmip : a toolbox for modeling and optimization in matlab," in *IEEE International Conference on Robotics and Automation (IEEE Cat. No.04CH37508)*, 2004, pp. 284–289.

[23] E. D. Andersen and K. D. Andersen, "The mosek interior point optimizer for linear programming: an implementation of the homogeneous algorithm," in *High performance optimization*. Springer, 2000, pp. 197–232.

[24] R. D. Zimmerman, C. E. Murillo-Sánchez, and R. J. Thomas, "Matpower: Steady-state operations, planning, and analysis tools for power systems research and education," *IEEE Transactions on Power Systems*, vol. 26, no. 1, pp. 12–19, 2011.

[25] O. Wasynczuk, S. Sudhoff, T. Tran, D. Clayton, and H. Hegner, "A voltage control strategy for current-regulated pwm inverters," *IEEE Transactions on Power Electronics*, vol. 11, no. 1, pp. 7–15, 1996.